Competing instabilities of rotating boundary-layer flows in an axial free-stream

Zahir Hussain

Competing instabilities of rotating boundary-layer flows in an axial free-stream

Zahir Hussain[1]*

ISROMAC 2016

International Symposium on Transport Phenomena and Dynamics of Rotating Machinery

Hawaii, Honolulu

April 10-15, 2016

Abstract

In this study, a new centrifugal instability mode, which dominates within the boundary-layer flow over a slender rotating cone, defined by half-angle $\psi < 40°$, is used for the first time to model the problem when an enforced oncoming axial flow is introduced. The resulting similarity solution represents the basic flow more accurately than previous studies in the literature. This mean flow field is subsequently perturbed leading to disturbance equations that are solved via numerical and analytical approaches, importantly yielding favourable comparison with existing experiments. Meanwhile, a formulation consistent with the classic rotating-disk problem has been successful in predicting the stability characteristics of broad rotating cones, defined by half-angle $\psi > 40°$, in axial flow.

Keywords

Rotating boundary-layer — crossflow instability — centrifugal instability — broad/slender rotating cone — co-rotating/counter-rotating spiral vortices

[1] *Division of Mathematics, School of Computing, Mathematics and Digital Technology, Manchester Metropolitan University, Manchester M1 5GD, United Kingdom*

*__Corresponding author__: Z.Hussain@mmu.ac.uk

1. INTRODUCTION

This article forms part of a series of studies which have used theoretical techniques to construct the correct models of governing instability for both broad and slender rotating cones. The current study represents a significant extension to the general problem in the slender cone case, introduced when enforcing an oncoming axial flow.

Physically, the problem represents an accurate model of axial airflow over rotating machinery components at the leading edge of a turbofan. In such applications, laminar-turbulent transition within the boundary layer can lead to significant increases in drag, resulting in negative implications for fuel efficiency, energy consumption and noise generation. Consequently, delaying transition to turbulent flow is seen as beneficial, and controlling the primary instability may be one route to achieving this. Ultimately, control of the input parameters of such a problem may lead to future design modifications and potential cost savings.

Our results are discussed in terms of existing experimental data and previous stability analyses on related bodies. Importantly, axial flow is seen to delay the onset of convective instability for both broad and slender rotating cones; the exact mechanism of interaction governing the transition process however is very different for both instabilities. Broad-angled rotating cones are susceptible to a crossflow instability visualised in terms of co-rotating spiral vortices, whereas slender rotating cones have transition characteristics governed by a centrifugal instability, which is visualised by the appearance of counter-rotating Görtler vortices. It is the relative competition of these two governing mechanisms that is explored in detail in this study, particularly with regard to the role of travelling modes in the breakdown process.

2. METHODS

We consider a cone of half-angle ψ rotating in a fluid of kinematic viscosity ν^* with an angular velocity Ω^* in an anti-clockwise direction around the streamwise coordinate axis x^* (where a * denotes a dimensional quantity in all that follows). We construct coordinate axes aligned along with and perpendicular to the spiral vortices ($\hat{x}^*$ and y^*, respectively), as shown in Figure 1. Further details of the relationship between the coordinate systems, including a required Mangler transformation, are provided in [5]. These are shifted from the conventional streamwise and azimuthal coordinates, x^* and θ, which are based on cylindrical polar coordinates. In such a problem, there exists a boundary layer close to the rotating cone surface characterised by the distance along the cone l^* and defined by the Reynolds number, R, such that:

$$\mathrm{R} = \frac{\Omega^* l^{*2} \sin\psi}{\nu^*}.$$

With the important distinction of the inclusion of the oncoming axial flow, the physical problem is subsequently altered such that there now exists a dimensional local slip velocity at the edge of the boundary layer, obtained via a well-known potential-flow solution (see for example [1]), given by $U_e = C^* x^{*m}$, where C^* is a constant.

We subsequently compare this velocity to the rotational velocity of the cone surface, given by $V_w = \Omega^* x^* \sin\psi$, to

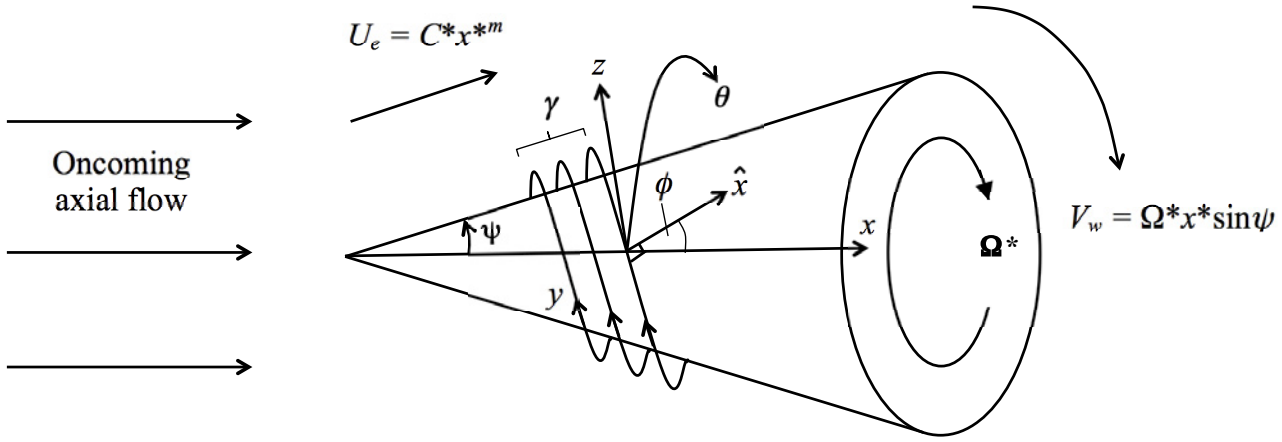

Figure 1. Diagram of the spiral vortex instability on a rotating cone placed in an oncoming axial flow, showing coordinates in the $\hat{x}$- and y-logarithmic spiral directions, as well as the corresponding vortex wavenumber, γ, and vortex waveangle, ϕ.

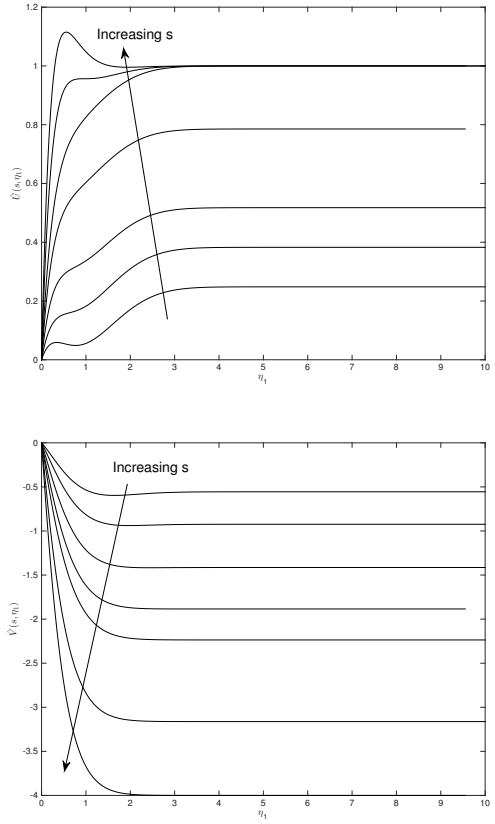

Figure 2. Velocity profiles $\hat{U}(s,\eta_1)$ and $\hat{V}(s,\eta_1)$ in the $\hat{x}$- and y-directions, respectively, at $\psi = 15°$ for $s = 1.5, 2, 3, 4, 5, 10, 16$ and $\phi(s) = 30.2°, 22.5°, 13.6°, 6°, 0°, 0°, 0°$ (in the directions of the arrows).

obtain an important ratio, which in part characterises the problem, known as the rotational-flow parameter, given by

$$s = \left(\frac{V_w}{U_e}\right)^2,$$

and used in [2, 3, 4]. In this study, we will use s to facilitate comparison of our results with experiments, as well as make reference to physical cases where the cone is rotating 'quickly' and the axial flow is increased from a zero value (ie. s decreasing from ∞), for example during the take-off phase of an aeroplane, once the rotating turbofans have reached an optimum rotational velocity.

Essentially, the boundary-layer flow undergoes competition between the streamwise flow component, due to the oncoming flow, and the rotational flow component, due to effect of the spinning cone surface, which can be described mathematically in terms of the control parameters, ψ and s. We present the results of convective instability analyses for the boundary-layer flow over broad and slender rotating cones in a variety of imposed axial flows, based on large Reynolds-number and short-wavelength asymptotics, as well as numerical solutions obtained via an Orr–Sommerfeld stability analysis.

Importantly, the basic flow quantities $\tilde{U}$ and $\tilde{V}$ are expressed as projections along the shifted spiral coordinates. However, due to the introduction of an oncoming axial flow, these are now functions of both the non-dimensional streamwise and surface-normal coordinates, x and z, respectively (where x is the streamwise direction over the cone, scaled on l^*). Hence, obtaining the base flows now require the solution of a system of PDEs (see [4] and [5] for full details and discussion) as opposed to the projected von Kármán solution of a system of ODEs presented in [6] for the still fluid problem. While there exist similar numerical basic flow for-

mulations used by [2] and [3], experimental verification of the basic flow is currently planned by R. Lingwood (personal communication, 2015).

At this point, we outline the important link between the standard surface-normal coordinate η and the modified surface-normal coordinate η_1 scaled on boundary-layer thickness according to the new velocity scales applied to the basic flow boundary-layer equations. The coordinate stretching yields

$$\eta_1 = \eta\Big(\frac{m+3}{2s^{\frac{1}{2}}}\sin\psi\Big)^{\frac{1}{2}}. \tag{1}$$

This relation enables the shifted velocity profiles $\tilde{U}(x,\eta)$ and $\tilde{V}(x,\eta)$, expressed in terms of the standard boundary-layer coordinates, to be written in terms of $f'(s,\eta_1)$ and $g(s,\eta_1)$, which depend on s and the modified boundary-layer coordinate. The shifted basic flow quantities are written correctly in the form:

$$\tilde{U}(x,\eta) = U(x,\eta)\cos\phi + V(x,\eta)\sin\phi,$$
$$\tilde{V}(x,\eta) = U(x,\eta)\sin\phi + V(x,\eta)\cos\phi.$$

Here, $U(x,\eta)$ and $V(x,\eta)$ can be expressed in terms of the solution functions $f'(s,\eta_1)$ and $g(s,\eta_1)$ (where $'$ indicates $\frac{\partial}{\partial\eta_1}$) obtained in [5] and presented in [4] for $\psi = 50°, 70°$. The numerical solutions for $f'(s,\eta_1)$ and $g(s,\eta_1)$ are obtained via the D03PEF NAG routine using a Keller box scheme and the method of lines. However, in this study, we remain consistent with the formulation presented in [5], pertaining to the shifted basic flow quantities, which are essential when considering the slender rotating cone problem for $\psi < 40°$. Specifically, we may write

$$\tilde{U}(x,\eta) = \frac{U_e}{\Omega^* l^* \sin\psi}\Big(f'(s,\eta_1)\cos\phi + s^{\frac{1}{2}}g(s,\eta_1)\sin\phi\Big) = s^{-\frac{1}{2}}\hat{U}(s,\eta_1), \tag{2}$$

$$\tilde{V}(x,\eta) = \frac{U_e}{\Omega^* l^* \sin\psi}\Big(f'(s,\eta_1)\sin\phi + s^{\frac{1}{2}}g(s,\eta_1)\cos\phi\Big) = s^{-\frac{1}{2}}\hat{V}(s,\eta_1), \tag{3}$$

where $\hat{U}$ and $\hat{V}$ are presented in Figure 2 for $\psi = 15°$ in a range of axial flows, increasing from $s = 1.5$ to $s = 16$ (corresponding to a 'quickly' rotating cone). We note that the $\hat{x}$-component, $\hat{U}$ exhibits a familiar inflexional nature, with its limiting value at the edge of the boundary layer increasing as s increases. However, for $s \geq 5$, we observe from the results of [3] that $\phi = 0°$, which is consistent with our basic flow solution where $\hat{U}$ recovers the streamwise basic flow component, f', to within a factor of $s^{-\frac{1}{2}}$. In contrast, the y-component of velocity $\hat{V}$ exhibits a uniform shear and is consistently reduced as s is increased.

We assume that the spiral waves are periodic in the $\hat{x}$-direction and introduce periodicity into the perturbation quantities of vortex $\check{x}$-wavenumber a and $\bar{y}$-wavenumber b. Scaling our perturbation quantities on the boundary-layer thickness, we introduce a combined flow of the form

$$\tilde{\mathbf{u}}^* = \Omega^* l^* \sin\psi[\{\tilde{U}(x,\eta),\tilde{V}(x,\eta),\mathrm{R}^{-\frac{1}{2}}W(x,\eta)\} + \mathrm{R}^{-\frac{1}{2}}\{\tilde{u}(\eta),\tilde{v}(\eta),\tilde{w}(\eta)\}\exp(\mathrm{i}a\check{x} + \mathrm{i}b\bar{y})].$$

Similarly, the pressure perturbation term scales as

$$p^* = (\rho^*\Omega^{*2}l^{*2}\sin^2\psi)\mathrm{R}^{-1}\tilde{p}(\eta)\exp(\mathrm{i}a\check{x} + \mathrm{i}b\bar{y}). \tag{4}$$

3. RESULTS AND DISCUSSION

3.1 Asymptotic analysis

We proceed to solve the governing disturbance equations (identical to those given in [5]) to determine leading- and next-order estimates of the scaled Taylor number for neutrally-stable modes, which arise due to the scaling analysis and loosely follows [7] for the Taylor problem of flow between concentric rotating cylinders. Importantly, we are able to form comparisons with results in the literature expressed in terms of Reynolds numbers. The corresponding Taylor number, which characterizes the importance of centrifugal to viscous forces, is given by

$$T = \frac{2\cot\psi\cos\phi}{\sin^4\psi}. \tag{5}$$

In the axial flow problem, for a fixed ψ, this quantity is an output of the analysis and represents a measure of how s affects the physical flow characteristics.

Upon incorporating the basic flow expansions, we expand the perturbation quantities and pose a WKB solution for small values of ϵ, where $a = \epsilon^{-1}$ for the wavenumber a in the $\check{x}$-direction. As for the still fluid problem, the dominant terms in the governing disturbance equations balance if we scale $T \sim \epsilon^{-4}$ and $W/V \sim O(\epsilon^{-2})$, resulting in identical perturbation expansions to those presented in [6] (reproduced here for clarity when manipulating subsequent quantities):

$$\begin{aligned}\tilde{u} &= E(u_0(\eta) + \epsilon u_1(\eta) + \epsilon^2 u_2(\eta) + \ldots),\\ \tilde{v} &= \epsilon^2 E(v_0(\eta) + \epsilon v_1(\eta) + \epsilon^2 v_2(\eta) + \ldots),\\ \tilde{w} &= E(w_0(\eta) + \epsilon w_1(\eta) + \epsilon^2 w_2(\eta) + \ldots),\\ T &= \epsilon^{-4}(\lambda_0 + \lambda_1\epsilon + \lambda_2\epsilon^2 + \ldots),\end{aligned}$$

where $\lambda = \lambda_0 + \lambda_1\epsilon + \lambda_2\epsilon^2 + \ldots$, $E = \exp(\frac{\mathrm{i}}{\epsilon}\int^{\varphi} K(\tau)\mathrm{d}\tau)$, $\varphi = \frac{\sin\psi}{\bar{h}_1}\eta$. and following [7], the growth K is a quantity to be determined.

After solving the leading- and first-order problems following [5] and scaling out various dimensional quantities, we obtain an estimate for the scaled effective Taylor number, which is given by

$$\bar{T} = \epsilon^{-4}\Big(\frac{2\sqrt{s}}{m+3}\Big)^{\frac{1}{2}}\Big[\frac{1}{\hat{V}'(s,0)} + \frac{2.3381\times 3^{\frac{1}{3}}}{|\hat{V}'(s,0)|}\epsilon^{\frac{2}{3}}\Big(\frac{\hat{V}''(s,0) + s^{-\frac{1}{2}}\hat{V}'(s,0)^2\cos\phi}{\hat{V}'(s,0)}\Big)^2 + \ldots\Big]. \tag{6}$$

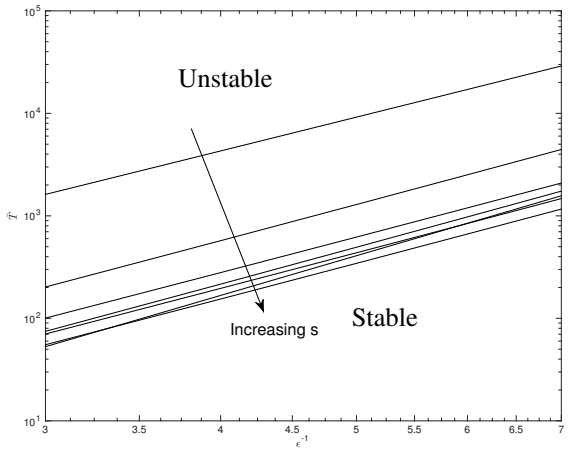

Figure 3. Asymptotic scaled Taylor number $\bar{T}$ as a function of non-dimensional vortex wavenumber ϵ^{-1} for $\psi = 15°, s = 1.5, 2, 3, 4, 5, 10, 16$ and $\phi(s) = 30.2°, 22.5°, 13.6°, 6°, 0°, 0°, 0°$.

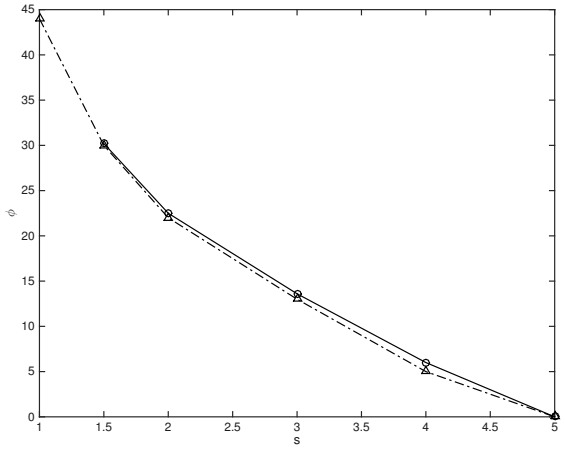

Figure 4. A comparison between the experimental observations of [3] (dot-dashed line, △) and the current theoretical predictions (solid line, ○) of the vortex orientation angle, ϕ, at the onset of instability. The diagram illustrates $\phi(s)$ reduces with increased rotational flow parameter, s, to a limiting value of $\phi = 0°$ at $s = 5$.

Logarithmic plots of the scaled asymptotic Taylor number against vortex wavenumber, $\epsilon^{-1} = a$, are shown in Figure 3 for $\psi = 15°$ and various values of s. We note that the asymptotic branches presented capture the effects of the leading- and first-order estimates for $\bar{T}$. The unstable region is above the curves and the stable region below. In general, we observe that increasing s leads to a trend of reducing the asymptotic Taylor number branch. Physically, this can be interpreted as promoting the more dangerous centrifugal instability mode, and hence destabilising the flow, which leads to a larger unstable region above the neutral stability branch, as depicted in Figure 3.

3.2 Numerical analysis

In this section, we develop the corresponding numerical solution, outlining the major differences between the axial flow problem formulated in this study and the still fluid case presented in [6]. These arise due to the fact that the basic flow quantities $\tilde{U}$ and $\tilde{V}$ are now functions of the logarithmic spiral coordinates $\check{x}$ and $\bar{y}$, as well as η. We manipulate the governing disturbance equations and subsequently express the basic flow terms in terms of η_1 by making use of the coordinate stretching (1). The analysis involves neglecting Coriolis terms and viscous streamline-curvature effects. Importantly, we note that the centrifugal mode under investigation differs from the streamline-curvature mode for large half-angle cones, which arises due to viscous effects of the cone surface. In contrast, the centrifugal mode for small half-angle cones arises from the centrifugal forces present in the mean flow for small ψ, owing to the effects of surface-curvature. Such centrifugal curvature terms are not neglected in the analysis and contain the Taylor number as a factor. Proceeding in this fashion yields a modified Orr–Sommerfeld (OS) equation for stationary disturbances within the system, given by

$$\left[\mathrm{i}\left(\partial^2_{\eta\eta} - k^2\right)^2 + \frac{Re}{\sqrt{s}}\left(\alpha_1\hat{U} + \beta_1\hat{V}\right)\left(\partial^2_{\eta\eta} - k^2\right) - \frac{Re}{2s}(m+3)\sin\psi\left(\alpha_1\hat{U}'' + \beta_1\hat{V}''\right)\right]\tilde{w} = 0, \qquad (7)$$

where

$$\alpha_1 = \frac{a\sin\psi}{Re}, \qquad \beta_1 = b\sin\psi, \qquad k = \sqrt{\alpha_1^2 + \beta_1^2}$$

represent the vortex wavenumbers in the $\check{x}$-, $\bar{y}$- and effective velocity-directions, respectively, and $\partial^2_{\eta\eta} = \partial^2/\partial\eta^2$. Furthermore, $Re = x\sin\psi$ is the local Reynolds number, interpreted as the local non-dimensional radius of the cone surface from the axis of rotation.

Importantly, we note from the basic flow profiles that for $s \geq 5$, the vortex activity is located at the wall, with the minimum of $\hat{V}'(s, \eta_1)$ existing at $\eta_1 = 0$. However, for $s < 5$, the curve has a minimum slightly departed from the wall, indicating the location of vortex activity will not be at $\eta_1 = 0$. This correlation results as a consequence of the requirement of obtaining valid real solutions for the growth rate K when solving the governing eigenvalue equation at leading order, which itself arises by following the study of [7] for the Taylor problem of flow between concentric rotating cylinders. For the case of $s < 5$, the solutions obtained are not the most dangerous modes available, but we include them as they provide useful information about non-zero wave angles (spiral waves) for a 15° rotating cone in axial flow. Furthermore, an interesting observation pertains to the related study of [8] on the rotating disk in axial flow, where non-

stationary travelling modes become more important as the strength of oncoming axial flow increases.

Indeed, the results of the numerical analysis are shown in figure 4, which presents the numerically calculated wave-angle, $\phi = \tan^{-1}(\beta_1/\alpha_1)$, versus various s for a 15° rotating cone. We compare results from the present study with the experiments of [3], observing close agreement. Both studies observe that in the regime of a 'quickly' rotating cone ($s > 1$), increasing s leads to a reduction in ϕ, to the point where $\phi = 0$ for $s \geq 5$, physically corresponding to the transition from spiral waves to circular or 'Taylor' vortices. Interestingly, this appears consistent with our basic flow and asymptotic solutions where for $s \geq 5$, the vortex activity remains located on the wall at $\eta = 0$. Conversely for $s < 5$, the stronger axial flow acts to sweep vorticity in the streamwise direction, which is again consistent with our asymptotic findings, namely that the vortex activity undergoes a slight departure from the wall in this regime.

Specifically, for $s < 5$ in the current problem, it appears that the location of vortex activity departing slightly from the wall suggests that travelling modes may grow as s is reduced and in fact become the most unstable modes in this parameter regime. Indeed, physically, the departure of a vortex from the wall suggests that vorticity within the boundary layer is no longer fixed on the cone surface, but is instead propagating or travelling in the effective velocity $\hat{x}$-direction. Ultimately, in order to confirm whether travelling instabilities may harbour the most unstable modes for the slender rotating-cone problem, a further investigation would be required, taking account of time-dependent terms within the governing disturbance equations.

In general, we observe close agreement between our asymptotic and OS numerical stability results, as well as with the numerical calculations of [2] (see [9] for comparisons of various slender cones with $\psi < 40°$). Importantly, while we have used the asymptotic results to provide an envelope for the right-hand branch of the numerical neutral stability curve, they are unable to predict the effect of varying axial flow on the critical Reynolds numbers. Nevertheless, the asymptotic analysis has proved invaluable in this study, as it reveals the correct length-scalings on which to model the counter-rotating vortex pairs, which characterise the centrifugal mode. Furthermore, by expanding the shifted basic flows about the location $\eta = 0$, we were able to confirm that the vortex activity of the most dangerous modes is located at the wall. Subsequently as s was varied, we tracked the location of vortex activity, observing that it departs slightly from the wall for $s < 5$. As a result, we have posed the hypothesis that stationary modes could dominate in the region $s \geq 5$, but below this non-stationary (or 'travelling') modes may begin to grow. Such an observation requires further investigation, but would not be possible through solely conducting a numerical analysis. Hence, the importance of an asymptotic analysis is clear in revealing the underlying physical mechanisms at work, along with how they might interact.

In contrast, the OS numerical stability results complement

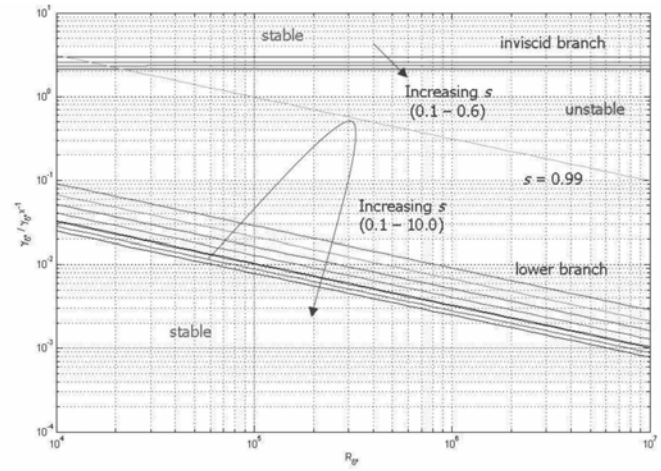

Figure 5. Plot of asymptotic neutral wavenumber predictions against rotational Reynolds number for inviscid type I and viscous type II modes for $\psi = 70°, s = 0.1 - 0.6$ (type I), $s = 0.1 - 10.0$ (type II). Increasing s shifts the curves as shown.

the asymptotics in confirming the existence of the neutral stability curve for the centrifugal mode. Furthermore, we observe a reduction in the critical Reynolds number Re_c as well as an increase in the critical amplification rate $\alpha_{1,c}$ with increasing s (see [9] for various slender cones with $\psi < 40°$). Hence, larger values of s are destabilising, suggesting that the centrifugal-instability mode is physically the most dangerous mechanism, despite alternatives being present, including the crossflow and Tollmien-Schlichting instabilities.

Ultimately, we propose a condition of 'optimal' stability existing around $s = 1$, where the competing effects of the rotational and streamwise flow components balance. For $s < 1$, the physical problem changes from a 'quickly' rotating cone (the parameter range considered in this study) to a 'slowly' rotating cone. In this regime, the physical effect of the oncoming axial flow strengthens, thereby promoting the streamwise Tollmien-Schlichting instability, which begins to dominate over the centrifugal mode. This optimal stability criterion of $s = 1$ appears to exist not only for the centrfiugal instability studied here, but also for the crossflow instability studied by [5] for a cone with $\psi = 70°$ rotating in an oncoming axial flow (see figure 5). The flow for both inviscid type I and viscous type II modes stabilises for increasing s, with $s = 1$ corresponding to the most stable flow setup in the type II case. Hence, for both flow instabilities on the rotating cone the findings predict an optimal stability criterion, which appears to be close to $s = 1$, where the effects of the two competing instabilities balance. This conclusion has interesting implications for the design of spinning projectiles, for example in military and defence applications. Here, the streamwise component is often large due to the projected velocity of the missile. For example, projectile applications that involve high rotation rates, such as spinning bullets and spinning missiles,

can spin up to 3000° per second and higher. In such case, it is important to design a missile that spins at sufficiently high rotation rate in order to promote the centrifugal mode and obtain a suitable balance between the competing instabilities. In fact, the primary instability can break-down to a secondary instability, which has been observed, for example, by [10] in the formation of 'horseshoe-like' vortices. Essentially, the aim in such spinning body applications is to reduce the parameter-scope for transition-to-turbulence within the flow. Therefore, influencing the primary and, potentially, the secondary instability, over a longer streamwise distance along the spinning body may achieve a delay in turbulent-transition, which consequently leads to more accurate targeting and projectile control properties. It should be noted at this point that the current study neglects the effects of compressibility, which would play a significant role in accurately modelling such high-speed applications.

ACKNOWLEDGMENTS

ZH wishes to acknowledge support from Manchester Metropolitan University.

REFERENCES

[1] L. Rosenhead. *Laminar Boundary Layers.* Oxford, 1963.

[2] R. Kobayashi. Linear stability theory of boundary layer along a cone rotating in axial flow. *Bull. Japan Soc. Mech. Engrs.* 4:934–940, 1981.

[3] R. Kobayashi, Y. Kohama and M. Kurosawa. Boundary-layer transition on a rotating cone in axial flow. *J. Fluid Mech.* 127:341–52, 1983.

[4] S. J. Garrett, Z. Hussain and S. O. Stephen. Boundary-layer transition on broad cones rotating in an imposed axial flow. *AIAA J.* 48, No. 6:1184–1194, 2010.

[5] Z. Hussain. Stability and transition of three-dimensional rotating boundary layers. PhD thesis, University of Birmingham, 2010.

[6] Z. Hussain, S. J. Garrett, and S. O. Stephen. The centrifugal instability of the boundary-layer flow over slender rotating cones. *J. Fluid Mech.* **755**, 274–293, 2014.

[7] P. Hall. Taylor-Görtler vortices in fully developed or boundary-layer flows: linear theory. *J. Fluid Mech.* **124**, 475–94, 1982.

[8] Z. Hussain, S. J. Garrett and S. O. Stephen. The convective instability of the boundary layer on a rotating disk in axial flow. *Phys. Fluids* **23**, 1141108, 2011. *J. Fluid Mech.* **124**, 475–94, 1982.

[9] Z. Hussain, S. J. Garrett, S. O. Stephen and P. T. Griffiths. The centrifugal instability of the boundary-layer flow over a slender rotating cone in an enforced axial free-stream. *J. Fluid Mech.* (to appear).

[10] Y. Kohama. Flow structures formed by axisymmetric spinning bodies. *AIAA J.* **23**, 1445, 1985.